COMMUNICATIONS: SIF Congress 2021

Study for a coherent denoising in unmodeled reconstruction of gravitational wave strain

A. Virtuoso([1])([2])

([1]) *Dipartimento di Fisica, Università di Trieste - Trieste, Italy*
([2]) *INFN, Sezione di Trieste - Trieste, Italy*

Summary. — I present a new method to remove detector noise from gravitational-wave (GW) interferometer data in the framework of unmodeled analyses, with special reference to *coherent WaveBurst* pipeline. The method introduces a pixel selection rule in the time-frequency representation of multidetector data to exclude noisy time-frequency components: this is performed multiplying each pixel by a weight function ranging from 0 to 1 and based on the coherence of the data among the detectors. Preliminary simulations indicate an improved suppression of noise with better reconstruction of both polarization components of detected GW signals.

1. – Introduction

To date, compact binary coalescences (CBC) are the only gravitational-wave sources that have been detected by the interferometers of the LIGO/Virgo/KAGRA (LVK) Collaboration, with both modeled and unmodeled pipelines [1]. Modeled pipelines [2,3] use matched-filters and large template banks to detect gravitational-wave signals from CBCs with optimal efficiency (highest signal-to-noise ratio), but also unmodeled pipelines can detect these signals [4]. Moreover, unmodeled (or, better, *weakly modeled*) pipelines are essential when searching for other sources of gravitational waves —like supernovae, neutron star glitches, cosmic strings and more [5]— where precise waveform models are missing. Although unmodeled pipelines cannot output the intrinsic model parameters, *e.g.* black hole spin, they can still be used to estimate some of the extrinsic parameters of the detected waves, such as their polarization content and sky localization, even when the signal source is unknown or theoretically not well understood.

In LVK Collaboration, the main unmodeled pipeline is *coherent WaveBurst* (cWB) [6]. Very schematically, cWB first decomposes each interferometer data into time-frequency (TF) representation using Wilson-Daubechies-Meyer (WDM) wavelets, and next it combines coherently these data into a likelihood function which is maximized with respect to sky location to detect the presence of a GW signal and, if so, to reconstruct it [7].

2. – The likelihood function

Having a network of K detectors, using $\mathrm{x}_k[i]$ to denote the amplitude from the k-th detector of the i-th pixel in the two dimensional TF representation, the vector of detector responses is

$$(1) \qquad \mathbf{x}[i] = \mathbf{F}_+(\theta, \phi)\mathrm{h}_+[i] + \mathbf{F}_\times(\theta, \phi)\mathrm{h}_\times[i] + \mathbf{N}[i],$$

where $\mathrm{h}_{+,\times}$ are the strains associated with the $+$ and $\times$ polarizations of the GW, $\mathbf{F}_{+,\times}(\theta, \phi)$ are the corresponding vectors of antenna patterns which depend on the source location (θ, ϕ), and $\mathbf{N}$ is the vector of detector noises. Data are whitened by dividing them by the amplitude spectral density $\sigma_k[i]$. A further simplification is achieved with a rotation in polarization space so that the normalized antenna patterns $\mathbf{f}_{+,\times}[i]$ ($\mathrm{f}_{k+,\times}[i] = \mathrm{F}_{k+,\times}/\sigma_k[i]$) are mapped to $\boldsymbol{f}_{+,\times}[i]$, which are orthogonal with respect to each other, *i.e.*, $\boldsymbol{f}_+[i] \cdot \boldsymbol{f}_\times[i] = 0$; this defines the so-called Dominant Polarization Frame (DPF)[1]

$$(2) \qquad \boldsymbol{w}[i] = \boldsymbol{f}_+[i]h_+[i] + \boldsymbol{f}_\times[i]h_\times[i] + \boldsymbol{n}[i],$$

where $\boldsymbol{n}[i]$ is the whitened noise. The whitened response $\boldsymbol{w}[i]$ is used to define a Gaussian likelihood function. cWB is based on the maximization of the log-likelihood ratio between signal (S) and background (B) hypothesis

$$(3) \qquad 2\ln \Lambda_{\mathrm{cWB}}(\boldsymbol{s}[i]) = \ln \left[p(\mathbf{x}[i]|S)/p(\mathbf{x}[i]|B) \right] = \boldsymbol{w}[i]^2 - (\boldsymbol{w}[i] - \boldsymbol{s}[i])^2,$$

where $\boldsymbol{s}[i]$ is the whitened reconstructed signal. The maximization of eq. (3) leads to the solution $\tilde{\boldsymbol{s}}[i] = \mathcal{P}[i]\boldsymbol{w}[i]$, where $\mathcal{P}[i]$ is the projector into the subspace defined by $\boldsymbol{f}_{+,\times}[i]$. Then $h_{+,\times}[i]$ can be obtained from $\tilde{\boldsymbol{s}}[i]$ solving the inverse problem, as done in [8].

The maximum of the likelihood ratio defines the main statistic used by cWB:

$$(4) \qquad \mathcal{L}[i] = 2\ln \Lambda_{\mathrm{cWB}}(\tilde{\boldsymbol{s}}[i]) = \boldsymbol{w}[i]^2 - (\boldsymbol{w}[i] - \mathcal{P}[i]\boldsymbol{w}[i])^2 = \boldsymbol{w}[i]^\dagger \mathcal{P}[i]\boldsymbol{w}[i].$$

Two related quantities, the *coherent energy*

$$(5) \qquad E_c[i] = \sum_{a \neq b} w_a^*[i]\mathcal{P}_{ab}[i]w_b[i] \quad a, b = 1, ..., K$$

and the *null energy*

$$(6) \qquad E_n[i] = (\boldsymbol{w}[i] - \tilde{\boldsymbol{s}}[i])^2 = (\boldsymbol{w}[i] - \mathcal{P}[i]\boldsymbol{w}[i])^2 = \boldsymbol{w}[i]^\dagger (\mathcal{I} - \mathcal{P}[i])\boldsymbol{w}[i],$$

where $\mathcal{I}$ is the identity matrix, are used to define the *correlation coefficient*

$$(7) \qquad cc[i] = |E_c[i]|/\left(|E_c[i]| + E_n[i]\right)$$

---

[1] Note that the polarizations are rotated as well, while each detector response and detector noise are rotation-invariant.

which estimates the coherence among different detectors: when $cc[i] \simeq 1$ ($|E_c[i]| \gg E_n[i]$) there is a high coherence and it is likely that signal is present in the i-th pixel, while when $cc[i] \simeq 0$ ($E_n[i] \gg |E_c[i]|$) data are incoherent.

3. – Coherent pixel selection for improved denoising

cWB implements a computationally fast denoising by selecting only pixels with sufficiently large energy $\boldsymbol{w}[i]^2$ [9]. I propose to take all the pixels, while weighting them with a function of an approximate likelihood ratio[2]. Assuming that the average correlation coefficient $\overline{cc}[i]$ over a small group of pixels surrounding $[i]$ in the TF map can be described as a (truncated) Gaussian random variable, I take $\langle \overline{cc}[i] \rangle = 0$ for the background hypothesis, and $\langle \overline{cc}[i] \rangle = 1$ for the signal hypothesis. So the two distributions are

$$(8a) \qquad p(\overline{cc}[i]|B) = \frac{1}{\sqrt{2\pi\sigma_B[i]^2}} \left[\frac{1}{2}\mathrm{erf}\left(\frac{1}{\sqrt{2}\sigma_B[i]}\right) \right]^{-1} \exp\left(-\frac{(\overline{cc}[i])^2}{2\sigma_B[i]^2}\right),$$

$$(8b) \qquad p(\overline{cc}[i]|S) = \frac{1}{\sqrt{2\pi\sigma_S[i]^2}} \left[\frac{1}{2}\mathrm{erf}\left(\frac{1}{\sqrt{2}\sigma_S[i]}\right) \right]^{-1} \exp\left(-\frac{(\overline{cc}[i]-1)^2}{2\sigma_S[i]^2}\right),$$

where the variances are $\sigma_S[i]^2 = (1/n)\sum_{j\in N}(cc[j]-1)^2$ and $\sigma_B[i]^2 = (1/n)\sum_{j\in N} cc[j]^2$, N is the set of neighboring pixels surrounding $[i]$ and n is their number. It is easy to see that the logarithm of the likelihood ratio $\mathcal{K}[i] = \log_{10} \Lambda_{\overline{cc}}[i]$, where $\Lambda_{\overline{cc}}[i] = p(\overline{cc}[i]|S)/p(\overline{cc}[i]|B)$, is a roughly linear function of $\overline{cc}[i]$ so that the following sigmoid function:

$$(9) \qquad \lambda(\mathcal{K}[i]) = \frac{1}{2}\left(1 + \mathrm{erf}\left[\alpha(\mathcal{K}[i] - \beta)\right]\right)$$

is closely related to the cumulative distribution function of $\overline{cc}[i]$; I then use $\lambda(\mathcal{K})$ to assign a weight to each pixel, utilizing the α, β parameters to fine-tune the selection. This method of pixel weighting is not yet implemented in cWB, however I have coded a toy implementation which performs well in simple tests, where a signal corresponding to a binary black hole coalescence[3] from a known source location is injected in simulated Gaussian noise for a three-detector network (*i.e.,* LIGO Livingston, LIGO Hanford, Virgo). Results are reported in fig. 1: after a basic tuning of α and β the proposed pixel selection rejects more noise than straightforward cWB-likelihood maximization. The improved quality of the reconstruction is quantified in the figure by the *overlap* between the injected and the reconstructed signals in time domain, defined by

$$(10) \qquad O_{+,\times}\left[\mathrm{h}_{+,\times}^{(in)}, \mathrm{h}_{+,\times}^{(re)}\right] = (\mathrm{h}_{+,\times}^{(in)}, \mathrm{h}_{+,\times}^{(re)})\bigg/\sqrt{(\mathrm{h}_{+,\times}^{(in)}, \mathrm{h}_{+,\times}^{(in)})(\mathrm{h}_{+,\times}^{(re)}, \mathrm{h}_{+,\times}^{(re)})},$$

where $(a,b) = \int_{t_{rs}} a(t)b(t)\mathrm{d}t$ is calculated over the time of the reconstructed signal t_{rs}.

---

[2] In a Bayesian frame with a uniform prior, the likelihood ratio is proportional to the posterior probability density function that the pixel contains energy from a true signal.
[3] I used the `SEOBNRv4_opt` approximant implemented within PyCBC to generate a GW170814-like event.
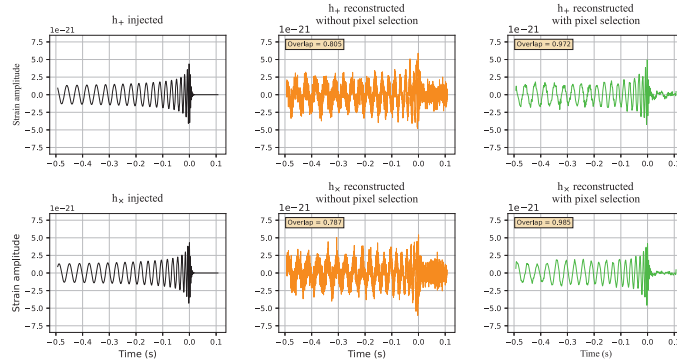
Fig. 1. – Comparison between injected polarizations (first column), polarizations reconstructed with no pixel selection (second column) and polarizations reconstructed with the pixel selection proposed in this work (third column). Here the weight function parameters are taken as $\alpha = 6$, $\beta = 0.4$. The method proposed here gives better overlaps (0.972 for h_+, 0.985 for $h_\times$) between injected and reconstructed polarizations compared to no pixel selection (*i.e.,* maximized Λ_{cWB} only, 0.805 for h_+, 0.787 for $h_\times$).

4. – Conclusions

This new proposed method performs well in ideal conditions, *i.e.,* with simulations involving Gaussian noise only, known source location of the detected signal and fine tuned parameters of the weight function. Future work will be devoted to test the method performances with respect to the current hard cuts: further tests will include larger set of signals from many different sky locations and real data. These tests should also provide guidance for an appropriate tuning of the weight function parameters.

* * *

REFERENCES

[1] ABBOTT R. *et al.*, *GWTC-3: Compact binary coalescences observed by LIGO and Virgo during the second part of the third observing run*, arXiv preprint, arXiv:2111.03606 (2021).
[2] USMAN S. *et al.*, *Class. Quantum Grav.*, **33** (2016) 215004.
[3] CANNON K. *et al.*, *SoftwareX*, **14** (2021) 100680.
[4] ABBOTT B. P. *et al.*, *Phys. Rev. D*, **93** (2016) 122004.
[5] ABBOTT R. *et al.*, *Phys. Rev. D*, **104** (2021) 122004.
[6] DRAGO M. *et al.*, *SoftwareX*, **14** (2021) 100678.
[7] KLIMENKO S. *et al.*, *Phys. Rev. D*, **93** (2016) 042004.
[8] DI PALMA I. and DRAGO M., *Phys. Rev. D*, **97** (2018) 023011.
[9] DRAGO M., *Search for transient gravitational wave signals with unknown waveform in the LIGO-Virgo network of interferometric detectos using a fully coherent algorithm*, PhD Thesis (2010).